PAPER • OPEN ACCESS
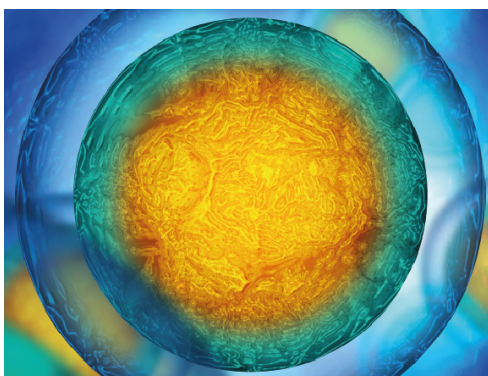
Get a grip: inward dactyl motions improve efficiency of sideways-walking gait for an amphibious crab-like robot

View the article online for updates and enhancements.

Bioinspiration & Biomimetics

Get a grip: inward dactyl motions improve efficiency of sideways-walking gait for an amphibious crab-like robot

N M Graf ⓘ, J E Grezmak* ⓘ and K A Daltorio ⓘ

Department of Mechanical and Aerospace Engineering, Case Western Reserve University, Cleveland, OH, United States of America
* Author to whom any correspondence should be addressed.

E-mail: nmg63@case.edu, jeg100@case.edu and kathryn.daltorio@case.edu

Abstract

Crabs are adept at traversing natural terrains that are challenging for mobile robots. Curved dactyls are a characteristic feature that engage terrain in order to resist wave forces in surf zones. Inward gripping motions at the onset of the stance could increase stability. Here, we add inward gripping motions to the foot trajectories of walking gaits to determine the energetic costs and speed for our 12 degree of freedom (DOF) crab-like robot, Sebastian. Specifically, we compared two gaits in which the step size (stance length) was the same, but the swing trajectories were either triangular (to minimize trajectory length) or quadrilateral (in which the leg deliberately oversteps in order to perform a distributed inward grip). The resulting gripping quadrilateral gait significantly outperformed the nongripping triangular gait on diverse terrains (hard linoleum, soft mats, and underwater sand), providing between 15% and 34% energy savings. Using this gait eliminates the advantage of spherical end effectors for slip reduction on hard linoleum, which may lead to a better understanding of how to use crab-like morphology for more efficient locomotion. Finally, we subjected the walking robot to lab-generated waves with a wave height approximately 166% of the dactyl length. Both gaits enabled the robot to walk undisturbed by the waves. Taken together, these results suggest that impact trajectory will be key for future amphibious robots. Future work can provide a deeper understanding of the relationships between dactyls, gaits, and substrates in biology and robots.

1. Introduction

Crabs have unique biological characteristics that allow them to inhabit both dry land and harsh aquatic environments, which have developed in multiple species, such as lobsters and crabs, through a process called carcinisation [1]. For example, crabs have developed tapered feet, or dactyls, which help them dig into granular media and grasp onto rocky substrates [1]. Crabs are dynamic animals, and different species have adapted to different environments [1–3], using a variety of gaits including forward walking [4], sideways walking [5], and punting [6]. While buoyant forces provide support to the crabs when submerged [7, 8], terrestrial crabs and hydrostatic land crabs tend to have a more rigid, over-designed body in order to better adapt to life on land [9]. Since crabs are the largest arthropods capable of transitioning between dry land and the large hydrodynamic forces in water [9], their strategies may be of value for amphibious robots.

Due to their numerous advantages in complex environments, other researchers have developed crab-inspired robots. Nguyen *et al* developed a compliant microgripper inspired by the profile of a sand bubbler crab [10]. Expanding on the gripping capabilities of crabs, Ma *et al* developed Crabbot which uses crab-like clamps to climb up poles [11]. Cha *et al* also took inspiration to the milli-scale with their milli-scale crab-inspired crawling robot [12]. Larger-scale autonomous legged underwater vehicles Ursula and Ariel have been developed for mine hunting in the surfzone [13]. The design of a leg–paddle-hybrid-driven robot and bounding gait inspired by swimming crabs was presented in [14]. *Chinese mitten crabs*

inspired Zhang *et al* to develop a compliant crab-like robot with an adaptive crab-inspired gait [15]. Similarly, *Pachygrapsus marmoratus* inspired Chellapurath *et al* to develop the underactuated SILVER 2.0 [16]. An even larger-scale crab-inspired robot is the car-sized Crabster CR200, which will be capable of lifting and storing objects [17]. While heavy robots can resist wave forces with weight, they often have higher energy costs, especially when walking in dry sand. Smaller robots, however, are more susceptible to being overcome by high-energy shore waves. For example, Krummel *et al* acknowledged their horse-shoe crab-inspired robot may be flipped by waves, and thus incorporated into the design a tail that acts as a self-righting mechanism [18]. Especially at smaller scales, an important question is how can the legs be best used to resist wave forces?

Our goal is to apply the distributed inward gripping strategy that climbing robots use to resist gravity to help crab-like robots navigate in surf and swash zones. Distributed inward gripping inspired by beetles helped a simple one degree of freedom (DOF) robot walk inverted on screens in 2008 [19]. Since then, other robots such as the surface grasper designs of Hawkes *et al* [20] and Palmer III *et al*'s DIGbot [21] have utilized this concept to demonstrate the ability to resist gravitational forces when climbing complex surfaces. Robots such as Spinyhand [22], RoboSimian [23], the Spiny Toe [24], the hybrid climbing robot [25], a bio-inspired wall-climbing robot [26], Li *et al*'s climbing robot [27], and a grappling-hook-like claw system [28] utilize spines to penetrate and attach themselves to climbing surfaces.

We have previously shown that using dactyl-inspired feet enables a crab-like robot to better resist wave forces. In addition, even in fine play sand, the robot can grab the ground, effectively increasing its effective body weight by a third [29, 30]. In compacted outdoor beach environments, the grip force may be even greater [31].

In this paper, we aim to determine the effects of incorporating the DIG strategy into walking gaits for a crab-like robot. Because we have previously demonstrated the benefits of sideways walking rather than forward walking for our crab-like robot, Sebastian (figure 1) [32], we solely focus on sideways gaits. Specifically, we implement two different alternating tripod gaits which differ in their swing path: one which minimizes swing path distance for a desired step height and lifting angle, and the other which alters the former's swing path to incorporate the DIG strategy. In our previous work [29, 30] we demonstrate the value of DIG for standing robots; here, we evaluate the effects of reapplying the grip while walking. The gaits are implemented on several terrain types, including both solid and granular media, as well as laboratory-produced wave environments. The robot's speed and cost of transport (COT) are used as metrics for comparing gait performance. Compared
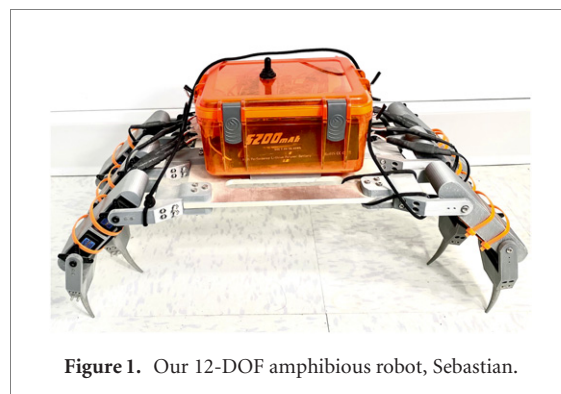

Figure 1. Our 12-DOF amphibious robot, Sebastian.

with previous work, the overall contribution here is two-fold: (1) the design of a gait path to apply DIG during walking, and (2) the experimental comparison of DIG-incorporated and traditional sideways walking gaits on several terrain types.

2. Related work

The relationship between foot trajectory and energy efficiency has been investigated for walking robots. Yang *et al* proposed a foot trajectory in the sagittal plane for a hydraulically actuated quadruped robot based on the Fourier series, which was shown to be more energy efficient than a trajectory based on cubic spline interpolation [33]. To minimize energy consumption in a hydraulically actuated quadruped, Kim *et al* proposed a foot rotation angle algorithm which planned the foot contact angle in the sagittal plane as a function of time [34]. Gao *et al* proposed a trajectory planning method for a forward-walking hexapod with passive compliant ankles based on polynomials with velocity and acceleration constraints [35]. The polynomial coefficients were determined to minimize impact forces and energy consumption. In this work, rather than optimizing foot trajectory for energy efficiency, we adopt an empirical approach to determine the relative efficiency of a gait with foot trajectories designed to incorporate the DIG strategy in granular media, which was not considered in the aforementioned studies.

Others have focused on developing models of foot impact dynamics of walking robots. Berges presented an energy-based approach for determining if a particular leg and foot configuration is capable of achieving no-slip and no-rebound impacts [36]. Mahapatra *et al* developed a full body analytical model for predicting the foot impact forces for a hexapod walking on hard uneven surfaces [37, 38]. These studies assume simple end effector models and are limited to hard or slightly deformable surfaces. In this work we are concerned with more complex interactions between dactyls and granular media, for which analytical models are intractable.

While other robots have demonstrated walking in granular media [39–42], our work starts from a goal

of not only walking efficiently in calm environments but also resisting perturbation forces. Others have shown that the angle of the foot with respect to the ground is important. For example, Li *et al* has shown for wheel-legged robots that impacting the ground with the curved portion of the c-shaped foot is better than reversing, the foot to impact with the pointed end [39]. Because our robot has more DOF per leg, we can more specifically control the entrance angles of the dactyls, potentially enabling new reduced actuation designs.

3. Amphibious robot development

3.1. Actuator selection
To walk in sand, actuators must be strong enough to move the legs through the increased resistance of the granular media but also light enough that the robot does not sink too deeply in the sand. For example, in our previous work, we had modified a lightweight tabletop robot [29, 30], but the servos often failed and had to be replaced due to overheating. Therefore, we examined the properties of 84 different servos, where the torque per mass ratio was prioritized for the design of the Sebastian robot.

Furthermore, servos that are already waterproofed are advantageous because they protect the internal components from sand and debris, and some have integrated heat sinks such that the robot can operate wet or dry without overheating.

Thus, the servo chosen for this work is the SAVOX SW2210SG-BE - Waterproof Premium, High Voltage, Brushless, Digital Servo (0.11 s/500 oz @ 7.4 V). These servos meet IP67 standards, which permit the servos to be operated in up to three feet of water for 30 min. This servo has a torque per mass ratio of 0.456, which outperforms both the plastic geared modified HEXY (0.278, [30]) and the metal geared modified HEXY (0.179, [29]). The operating range of this servo is 130°. The crab leg's workspace consists of $-80°$ to $20°$ for θ_1 and $-130°$ to $0°$ for θ_2 (figure 2). This range and workspace is the same as defined in [32, 43].

3.2. Dactyl and robot design
We have previously shown (on dry substrates) that sideways walking is more efficient than forward walking [32], which means only two DOF per leg are needed for straight line walking. Here, we updated the segments that house pairs of servos for each leg so that the entire 12-DOF robot (figure 1) can walk underwater or on dry substrates. With legs fully extended the wingspan is 73.7 cm. The body plate of the robot is made out of 6.35 mm thick aluminum, and the other components besides the body were 3D printed (Makergear M2, 100% infill for all but the mid legs that housed the servos, which were printed at 70% infill). In order to have Sebastian sink in the tank for submerged tests, approximately 100 g was added

inside the body of the robot. All of the testing in this work was conducted with the additional mass. With the additional mass, the final Sebastian robot has a mass of 4.36 kg. During an alternating tripod gait with three legs on the substrate, each leg supported an average weight of 1.37 N wet and 13.9 N dry.

3.3. Electronic layout of carapace
The robot's body, or carapace, which is a waterproof box (Outdoor Products translucent polycarbonate, $82.55 \times 133.35 \times 171.45$ mm) is where all of the electronic components besides the servos are stored. The internal components of the carapace consist of a Raspberry Pi 4B (8 GB RAM) powered by a PiSugar2 Pro (5000 mAh UPS Lithium Battery Power Module Platform), Pololu Maestro Servo Controller, Zeee Lithium Polymer battery (5200 mAh, 7.4 V), and an INA260 Power Sensor. The servos are powered with the lithium ion battery in the front of the carapace. The sensor has an Arduino Nano that communicates with the on-board computer to collect measurements of the current and power draw of the servo battery. The back of the bread board that connects the sensor and Arduino is coated in liquid electrician's tape (Starbrite). This sensor, along with the servo controller, is fixed to the back wall of the carapace.

3.4. Waterproofing methods
Servo extension wires (MoTrent 3-Pin Extension Cable) were attached to each of the 12 servos. This connection was reinforced by silicone (Gorilla's Clear Silicone Sealant) and shrink tube (Wirefy Heat Shrink Tubing 9.5 mm (recovered diameter of 3.2 mm)). The wires connecting the servos to the servo controller are fixed in place and waterproofed with more of the silicone sealant.

4. Gait development

With two parallel-axis revolute joints per leg, the dactyls have a reachable workspace defined in a plane perpendicular to the joint axes (shown in figures 3(B) and (D)). Within this space, a gait is defined by the closed path traced by the tip of the dactyl during a gait cycle. While dynamic gaits can be more energy efficient than static gaits for certain speed ranges (as observed for some quadruped animals [44]), here we focus on static gaits; specifically, all gaits are alternating tripod gaits, in which the front left, rear left, and middle right legs of the hexapod are out of phase with the other three legs [45]. The gait cycle can be divided into stance (when the dactyl is on the ground) and swing (when the dactyl is off the ground). For alternating tripod gaits, swing and stance are typically designed to have the same period (to achieve a duty factor of 0.5), although six-DOF hexapods such as SandBot [39] have used varying duty factors. These gaits are consistent with biological
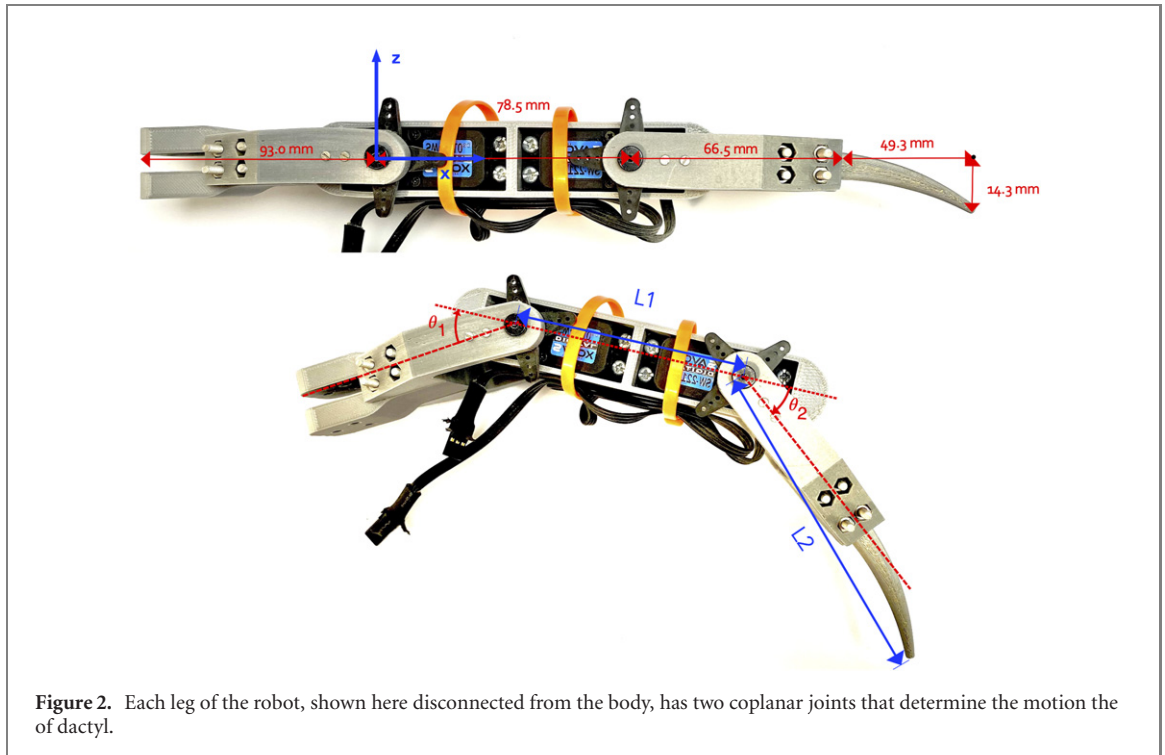
Figure 2. Each leg of the robot, shown here disconnected from the body, has two coplanar joints that determine the motion the of dactyl.

hexapods, who often use the same static gaits with variable duty factors [46], and furthermore, because there are always multiple legs on the ground, opposing forces can be applied.

Here, rather than simply raising the dactyl up and down during swing, our goal is to combine walking with DIG (which we have previously shown to be effective in climbing [19] and in increasing the effective weight in sand [29, 30]). We do this by changing the gait path during the swing phase. To enable control over the path geometry, as well as the speed at which the dactyl tip traces a path, inverse kinematics is used to compute the joint angles required for the dactyl to be positioned at several points along the desired path. Referring to a coordinate system with y-axis coincident with the knee joint axis (figure 2), the x and z positions of the dactyl tip are given as

$$x = L_1 \cos \theta_1 + L_2 \cos(\theta_1 + \theta_2) \qquad (1)$$

$$z = L_1 \sin \theta_1 + L_2 \sin(\theta_1 + \theta_2), \qquad (2)$$

where L_1 and L_2 are the segment lengths, and θ_1 and θ_2 are the joint angles as defined in figure 2. For a given position along the path, the corresponding joint angles can be obtained from equations (1) and (2) as

$$\theta_1 = \tan^{-1} \frac{z}{x} \mp \tan^{-1} \frac{L_2 \sin \theta_2}{L_1 + L_2 \cos \theta_2} \qquad (3)$$

$$\theta_2 = \mp \cos^{-1} \frac{x^2 + z^2 - L_1^2 - L_2^2}{2 L_1 L_2}. \qquad (4)$$

To avoid positive (outward) angles at the ankle joint (which may result in undesirable leg orientations for walking), only the negative solution in equation (4)

is considered, and only the negative solution in equation (3) is considered for the knee joint angle.

Starting from a set of waypoints defining key locations of the path (e.g. start and end points of the stance motion, peak raising height, etc), a gait path is created by solving for the joint angles according to equations (3) and (4) for several evenly spaced points on straight lines connecting the waypoints.

Using this method, two gait paths, TDP and QDP, are created to examine the effects of a swing path that incorporates an inward gripping motion on the robot's locomotive performance. The main difference is that the QDP includes not only a raise and lowering phase in the swing, but also a new grip phase. These two gait paths, along with the method for translating these gait paths to coordinated gaits, are described in detail below.

4.1. Triangular dactyl path (TDP) gait

The TDP gait serves as the baseline gait for which similar gaits with different swing paths can be built upon and compared. Thus, the TDP stance waypoint locations are chosen such that swing paths which travel beyond these waypoints in the x-direction can be accommodated. Additionally, the waypoint locations must allow the dactyls to raise high enough to be removed from loosely packed granular media during swing while remaining within the workspace.

The z position of stance ($z = -17.4$ cm) was chosen based on [32], because lowering the height makes a more sprawled posture difficult to support, and raising the height reduces the range of motion available in the workspace. For the front dactyl, stance begins at a waypoint at $x = 5.85$ cm and $z = -17.4$ cm (3f in figure 3), which positions the dactyl a distance
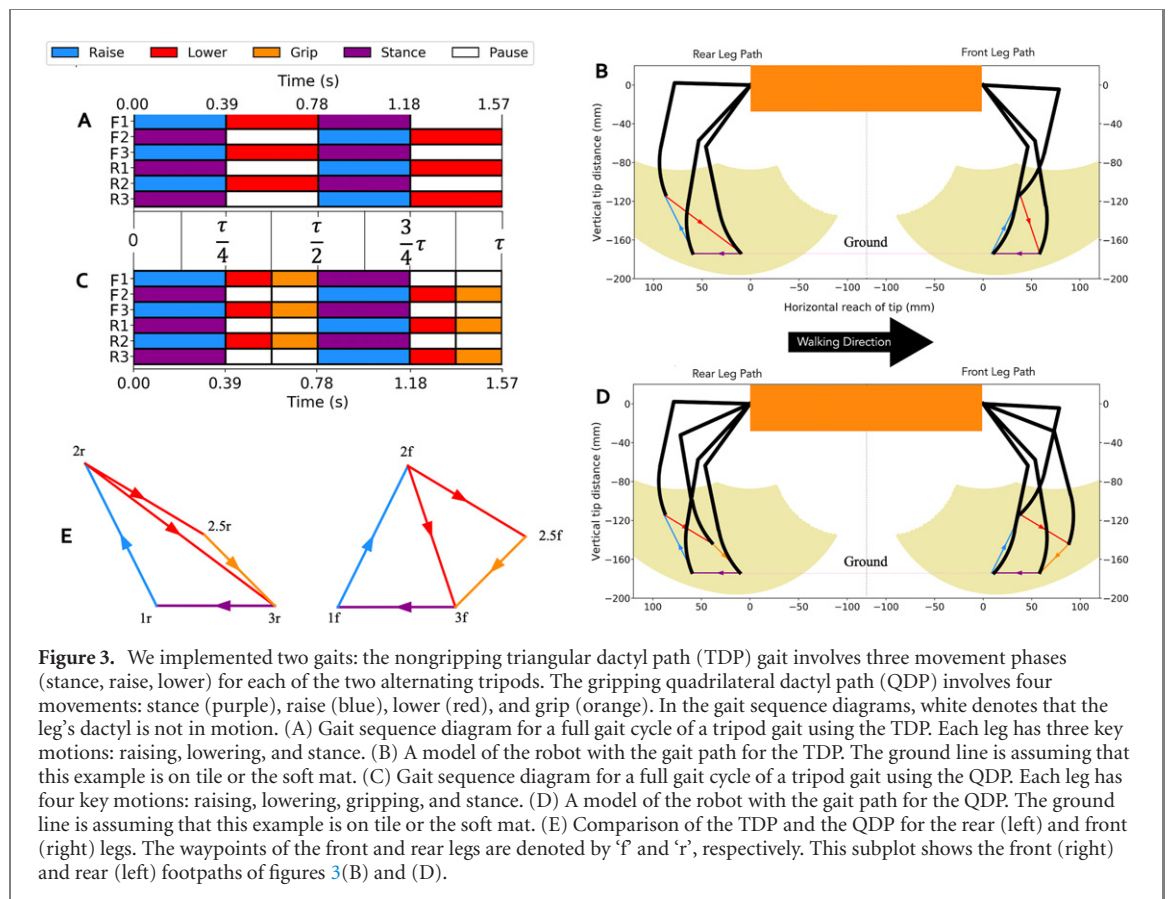
Figure 3. We implemented two gaits: the nongripping triangular dactyl path (TDP) gait involves three movement phases (stance, raise, lower) for each of the two alternating tripods. The gripping quadrilateral dactyl path (QDP) involves four movements: stance (purple), raise (blue), lower (red), and grip (orange). In the gait sequence diagrams, white denotes that the leg's dactyl is not in motion. (A) Gait sequence diagram for a full gait cycle of a tripod gait using the TDP. Each leg has three key motions: raising, lowering, and stance. (B) A model of the robot with the gait path for the TDP. The ground line is assuming that this example is on tile or the soft mat. (C) Gait sequence diagram for a full gait cycle of a tripod gait using the QDP. Each leg has four key motions: raising, lowering, gripping, and stance. (D) A model of the robot with the gait path for the QDP. The ground line is assuming that this example is on tile or the soft mat. (E) Comparison of the TDP and the QDP for the rear (left) and front (right) legs. The waypoints of the front and rear legs are denoted by 'f' and 'r', respectively. This subplot shows the front (right) and rear (left) footpaths of figures 3(B) and (D).

of 3.0 cm from the outer edge of the workspace in the x-direction, providing adequate space available for gaits which overstep during swing. Space is needed in the x-direction for front legs in QDP gait and for rear legs in both gaits. Stance ends at waypoint 1f at $x = 0.85$ cm and $z = -17.4$ cm, moving the dactyl a horizontal distance of 5.0 cm relative to the body. Thus on a no-slip substrate, each step would result in the body moving forward 5.0 cm. The robot begins the swing by lifting the dactyl in a direction tangent to the curve of the dactyl to waypoint 2f at $x = 3.85$ cm and $z = -11.4$ cm. In other words, rather than lifting the dactyl straight vertically, the dactyl moves outward along a slope with rise twice run. This allows the dactyls to be removed from granular media with minimal resistance. Specifically, the length of stance chosen as 5.0 cm causes the dactyls to be extracted at angle tangent to the dactyl itself at the end of stance when lifting to a vertical distance of 6.0 cm (corresponding to a z position of -11.4 cm), which is needed to guarantee the dactyls are fully extracted with minimal resistance in granular media. Finally, the gait path is completed by returning to the stance beginning waypoint.

The rear dactyls also point inward, so the leg motions are mirrored and modified for the dactyls pointed in the direction of motion. Thus, stance begins at the proximal waypoint 3r (corresponding to waypoint 3f for the front legs) and continues 5.0 cm to the distal waypoint 1r. Then the dactyl is

extracted again tangent to the dactyl at the same angle (to waypoint 2r at $x = 8.85$ cm and $z = -11.4$ cm). Again, the gait path is completed by returning to the stance beginning waypoint.

Thus, both forward and rear legs have the same step length (5.0 cm), height (6.0 cm), and angle of extraction (63°), with the entrance angle determined by the third side of the triangle.

4.2. Quadrilateral dactyl path (QDP) gait

In the QDP gait, the front and rear legs share stance waypoints with the TDP gait, as well as the waypoints defining the locations of the peak swing height. The difference is that an extra waypoint is included to allow the dactyls of both legs to move inwards toward the body at the same speed at the end of the swing phase, emulating the DIG strategy. For the front legs, this extra waypoint is located at $x = 8.85$ cm and $z = -14.4$ cm (2.5f), which positions them 3.0 cm from the stride starting waypoint in both the x- and z-direction. The resulting path from this waypoint to the stride starting waypoint, referred to as the 'grip', corresponds to the front legs deliberately overstepping before pulling the dactyls inwards to start the next stride. For the rear legs, the waypoint is located at $x = 3.85$ cm and $z = -14.4$ cm (2.5r), resulting in a grip distance equal to that of the front legs.

The grip distance of 3.0 cm horizontally corresponds to the small grip in our previous work, which added an effective 25% to the weight in submerged sand [29, 30].
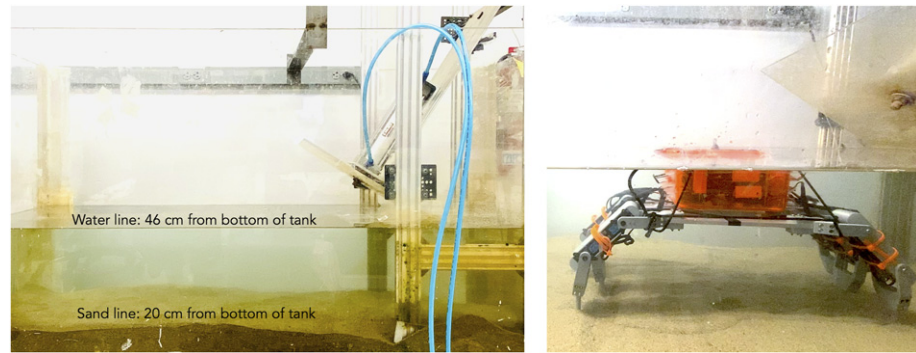
Figure 4. The wave tank is 156 cm × 66.5 cm × 92.0 cm. The bottom edge of the wave generator plate touches the waterline with the plate oriented at 60°. The water is 26 cm deep from the sand. Our Sebastian robot on the right is at the starting point for a submerged test.
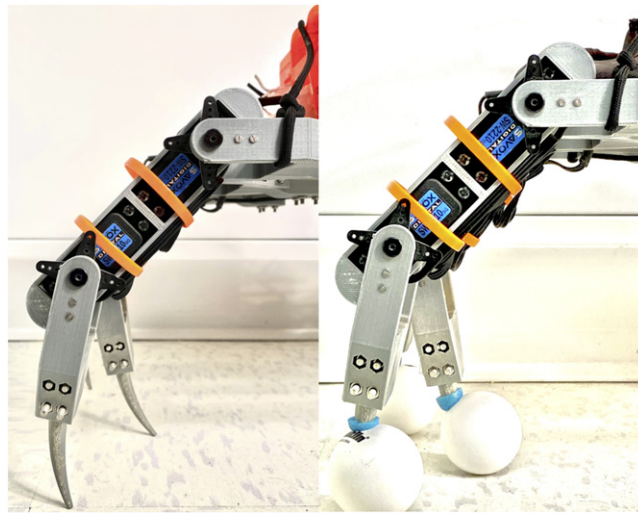
Figure 5. Dactyl (left) and ball (right) feet for Sebastian robot on tile substrate.

4.3. Control strategy

The gait paths discussed in the previous sections define the sequence of dactyl positions for each leg during a gait cycle. To translate these gait paths to individual leg trajectories that result in alternating tripod gaits, the controller follows the gait sequence diagrams in figures 3(A) and (C). In the first quarter-cycle, the front tripod (consisting of the outer two front legs and middle rear leg) raises while the opposing (rear) tripod completes the stance motion. The rear tripod then pauses while the front tripod completes the swing phase over the next quarter-cycle. For the QDP, the dactyls move to the waypoints defining the start of the grip path (2.5f and 2.5r for front and rear legs, respectively) over half of the quarter-cycle, and subsequently to the 3f and 3r waypoints over the next half of the quarter-cycle (figure 3(E)). The pausing of the rear tripod allows the front tripod to perform the grip with the front and rear leg dactyls moving at the same speed relative to the terrain. The same process is then carried out with the role of each tripod switched to complete the gait cycle.

As previously stated, joint angles are solved for several evenly spaced points on straight lines connecting the waypoints. By using an equal number of points between each waypoint, and using a constant time step between updates of the joint positions by the controller, the dactyl tips move between waypoints at constant speeds determined by the desired cycle period.

5. Experimental methods

5.1. Detailed experiments

The robot is wet-tested in our lab's wave tank, in which play sand with depth 20 cm is covered with water of depth 46 cm. This water depth is chosen to completely submerge the robot's legs, but leave the top of the robot in air to facilitate wireless communication. We choose to test in submerged sand rather than dry or moist sand because this is the most critical environment for resisting wave forces, and because submerged sand has consistent water content (rather than drying out over time).
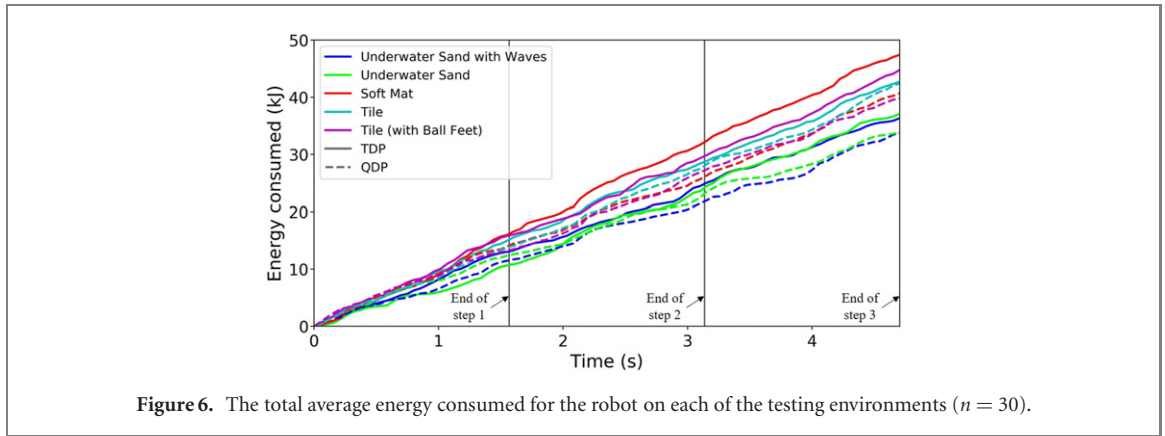
Figure 6. The total average energy consumed for the robot on each of the testing environments ($n = 30$).
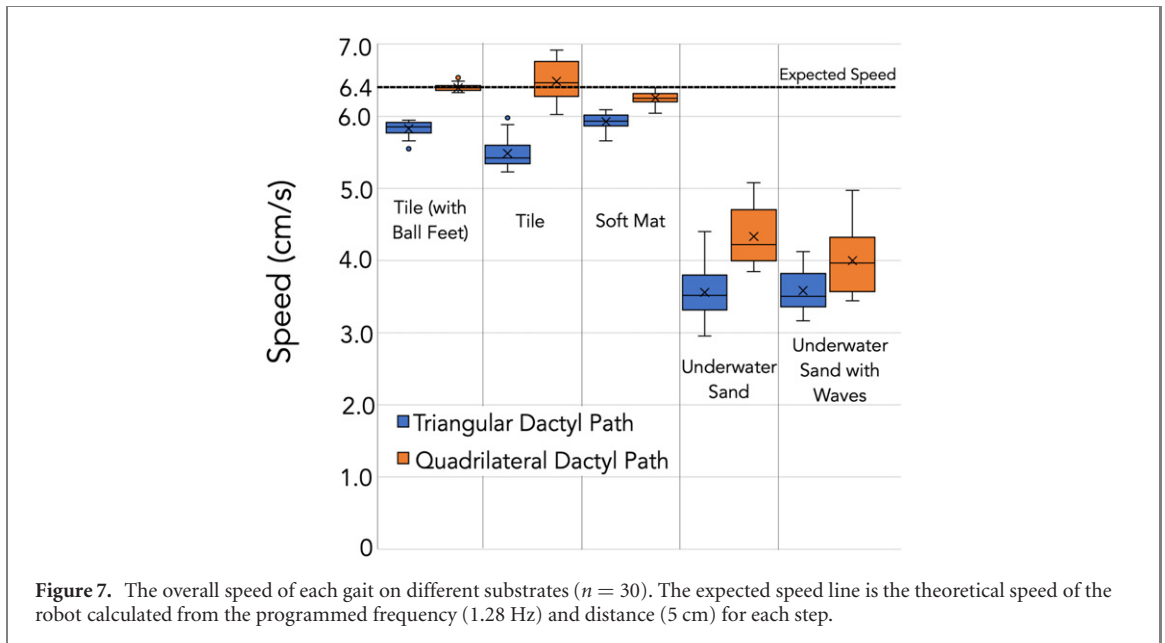

Figure 7. The overall speed of each gait on different substrates ($n = 30$). The expected speed line is the theoretical speed of the robot calculated from the programmed frequency (1.28 Hz) and distance (5 cm) for each step.

The robot is tested dry on hard linoleum tile floors and on a high friction surface (soft mat, TopPlus Yoga Mat: 72' by 24' Purple Thermoplastic Elastomer, 1/4 inch). The tests on the tile and soft mat serve as a control to examine how the sand effects the QDP and TDP gaits.

For each test, the robot is placed at the same starting point. In dry environments, the robot performs a set of four steps, and the robot's total horizontal travel distance is measured with a tape measure. In the submerged tests, the robot is placed into the testing platform shown in figure 4 and walks sets of three steps. Note that three steps keeps the robot in the optimal wave zone in our small indoor tank. A camera is used to record videos from a top down view of the robot, from which the robot's position over time is measured with Tracker (https://physlets.org/tracker/) by tracking the location of the power switch on the carapace which is a high contrast visible target. The robot's power consumption is measured with an onboard power sensor connected to the battery

powering the servos. Note that this will not include computational costs since the Pi has its own power source.

The robot's COT during each trial is found with equation (5) [47].

$$\text{COT} = \frac{E}{mgd} = \frac{P}{mgv}. \tag{5}$$

The gravitational acceleration, g, is constant, and the mass, m, is measured before testing. The horizontal travel distance, d, and velocity, v, are measured and calculated between trials. The power sensor records the power, P, used by the robot during each trial at 25 Hz, from which the total energy consumed while the robot is walking is computed. The computed energy consumption and measured travel distance are used to compute the COT according to equation (5). The COT is used as a metric for comparing the gait performances on different terrains, and because the resulting value is dimensionless, it can be compared across platforms or with our previous work [32].
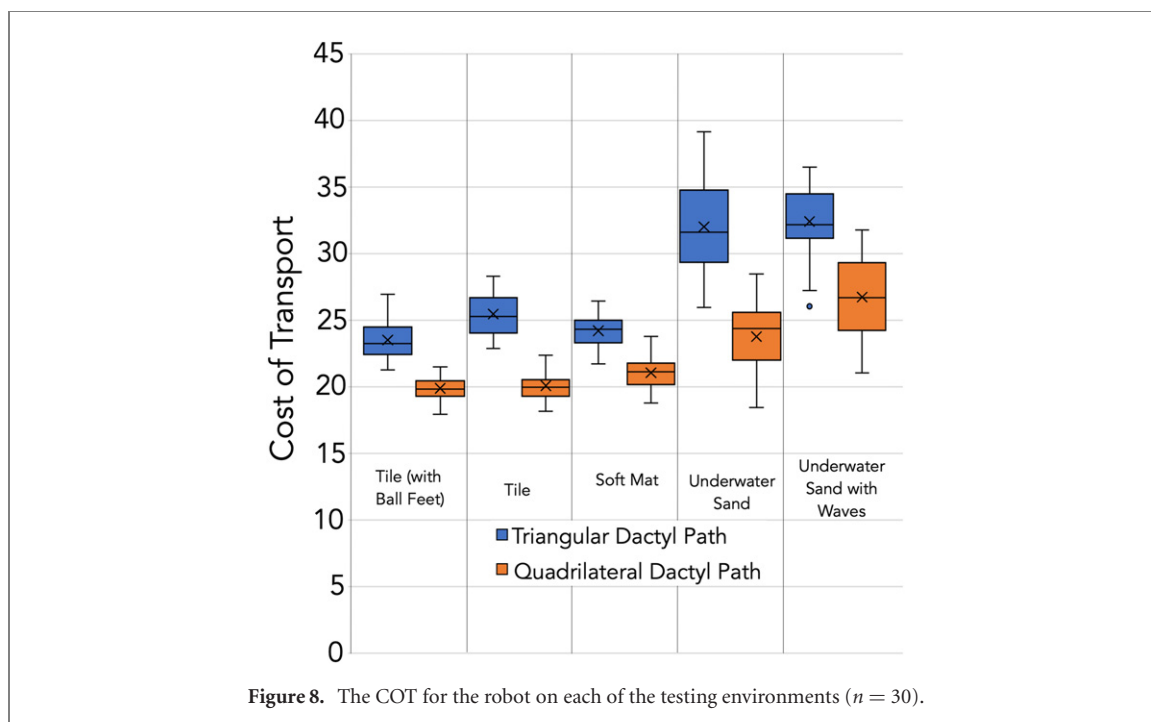
Figure 8. The COT for the robot on each of the testing environments ($n = 30$).

Finally, to determine the degree to which the dactyl shape influences performance, a set of control tests are performed with small hollow ping-pong balls covering the dactyls (figure 5). Examples of the different tests can be found at supplementary material.

5.2. Wave characterization

The wave tank (figure 4) in the lab has an acrylic board attached to a piston locked in place by a frame. The piston pumps the board up and down, causing waves to form in the tank. The period of the waves in the tank is 3.6 s, which was obtained by tracking the progress of the wave peak of one push of the piston with Tracker. The board pulls up after 2.8 s (the length of time it takes for the wave to reflect off of the opposite wall and reach the piston again) and pushes down again 0.8 s later (the length of time to reflect off of the nearer back wall and reach the piston) in order to keep a constant period of 3.6 s. The piston is initially pressurized at 100 psi and is run for five waves. The waves generated by this method are 8.19 cm above the water line (166.2% of the dactyl length). A gait period of 1.57 s was chosen to permit extra time between the waves if needed.

6. Results

We have recorded the energy consumed throughout the tests, as shown in figure 6, which shows that the rate of energy consumption is even throughout the duration of the three steps. We had expected that gripping might have a energetic cost. However, our gripping gait QDP outperformed the nongripping TDP gait in both speed and COT on each substrate,

as shown in figures 7 and 8, respectively. These are the results of 30 trials for each substrate and gait combination. The average speeds and standard deviations for TDP and QDP are shown in tables 1 and 2. These results suggest that a strategy of 'overstepping', especially with the front dactyls, in order to pull inward is useful on all substrates.

We can compare the actual speeds with the predicted speed (path step size times the step frequency, the horizontal line in figure 7). While the QDP speeds are typically close to the expected speed, the TDP speeds are only 85% of the expected speed on the tile floor. This suggests that the onset of swing is creating braking forces that are causing backward slip.

6.1. Effect of end effector shape

To determine to what extent the backwards slip is unique to the dactyl shape, we compare the tile results with balls covering the dactyls. In our prior work, replacing blunted feet with the same-shaped pointed dactyls halved our robot's speed on the same tile floor, even at the lowest speeds (figure 10(A), [29]). However, at that time we had not modified the gait to suit dactyls. Here, with the QDP gait, the dactyls can walk as fast as on the ball feet with both of them approximating the expected speed. The dactyls do have more variability, likely because the balls can handle rotations more smoothly.

With the TDP gait, both balls and dactyls are sensitive to the touchdown angle. While the balls lose 9% of the speed, the dactyls lose 15% of the speed on tile floors. This suggests that dactyls are particularly sensitive to appropriate touchdown angle. Thus, while Sebastian with the TDP gait is better than our previous robot, the QDP gait is even better.

Table 1. Average speeds and standard deviations in cm s^{-1}. The percent decrease is $(1 - \frac{\text{TDP}}{\text{QDP}}) \times 100$. The p-value is proof that the TDP nongripping gait is significantly slower than the QDP gripping gait on each substrate tested.

	TDP Avg speed $\pm$ SD	QDP Avg speed $\pm$ SD	Decrease with TDP	Comparison of gaits p-value
Tile (with ball feet)	5.83 ± 0.099	6.40 ± 0.050	9%	2.54×10^{-15}
Tile	5.49 ± 0.20	6.48 ± 0.27	15%	2.20×10^{-16}
Soft mat	5.93 ± 0.098	6.26 ± 0.89	5%	1.79×10^{-13}
Underwater sand	3.56 ± 0.35	4.33 ± 0.39	18%	1.68×10^{-10}
Underwater sand with waves	3.58 ± 0.27	4.00 ± 0.44	11%	0.001 38

Table 2. Average COTs and standard deviations. The percent decrease is $(\frac{\text{TDP}}{\text{QDP}} - 1) \times 100$. The p-value is proof that the TDP nongripping gait is significantly more expensive than the QDP gripping gait on each substrate tested.

	TDP Avg COT $\pm$ SD	QDP Avg COT $\pm$ SD	Increase with TDP	Comparison of gaits p-value
Tile (with ball feet)	23.9 ± 1.2	19.9 ± 0.86	20%	2.20×10^{-16}
Tile	25.5 ± 1.6	20.1 ± 1.0	27%	2.20×10^{-16}
Soft mat	24.2 ± 1.2	21.1 ± 1.2	15%	6.34×10^{-11}
Underwater sand	32.0 ± 3.5	23.8 ± 2.5	34%	2.19×10^{-13}
Underwater sand with waves	32.4 ± 2.5	26.7 ± 2.8	21%	1.39×10^{-8}

6.2. Effect of friction

Because we expect that the differences are due in part to slip, it is not surprising that the high friction substrate reduces the loss of speed associated with the TDP gait to 5%, and also narrows the spread of the data in each category. In general, greater slip also correlates with less energy costs, and greater energy cost savings associated with switching from TDP to QDP (27% savings for low friction and only 15% savings for high friction). This is likely because the gripping gait involves an intentional amount of inward motion against the ground.

6.3. Effect of underwater environments

As with previous work [29, 30, 32] walking in sand reduces the locomotion speed. However, while in our previous paper the sand speed was less than 40% of the tile speed, here the average sand speed is 67% of the tile speed. Furthermore, walking in sand is similarly sensitive to the touchdown angle, with a reduction in speed of 18% associated with TDP gaits.

Because walking on granular media can be particularly energetically expensive, it is especially helpful that switching from TDP to QDP results in a 34% COT saving. As shown in the accompanying video, the dactyls sink more deeply into the sand with QDP. For example, the front leg F2 in figures 3(A) and (D) penetrates approximately 5 mm (10% of the dactyl) deeper with QDP than when utilizing the TDP. As a result, the front legs F1 and F3 oscillate back and forth, indicating that there may not be as complete an anchor.

Additionally, we added waves to increase the similarity to the natural environment of shore crabs. Waves that were sufficient to shift our previous robot did not significantly affect the walking speeds of this

Figure 9. Sebastian robot in outdoor grassy walking speed test.

robot. As shown in our previous paper ([29] figure 8), the sand around the dactyls can wash away after multiple waves, and thus stepping can help the robot reanchor.

6.4. Effect of speed

Finally, the effect of walking speed on the relative performance of TDP and QDP gaits is investigated by changing the designed gait period. For a similar robot configuration, simulation studies have found that energy cost due to heat emissions tends to increase as speed decreases [46]. To test if the benefits of the QDP gait could still be observed at lower speeds, an additional experiment was performed in which the robot walked 30 steps outside in grass (figure 9) with the TDP and QDP gaits at their original (1.57 s) and at twice the original (3.14 s) gait periods. The results of each gait and period combination are shown in table 3.

As expected, increasing the gait period increases the COT for both the TDP and QDP gaits. However, the difference between them only slightly decreases, and the robot was still able to travel farther at a cheaper rate when using the QDP gait. This shows that the improved performance is due to the difference in gait rather than the speed.

Table 3. Average distance traveled, energy consumed, and COTs with standard deviations. Three trials of 30 steps were performed for each gait on an outdoor grass terrain.

	TDP		QDP	
	$1 \times$ speed	$0.5 \times$ speed	$1 \times$ speed	$0.5 \times$ speed
Avg distance traveled (m)	2.47 ± 0.03	2.44 ± 0.01	2.83 ± 0.02	2.82 ± 0.03
Avg energy used (J)	2730 ± 25.1	3700 ± 28.9	2905 ± 63.2	4050 ± 34.3
Avg COT	27.6 ± 0.15	38.0 ± 0.16	25.7 ± 0.71	36.0 ± 0.52

7. Conclusions and discussion

In this work, our robot Sebastian (figure 1) was evaluated for the first time in amphibious environments where gripping the ground may provide additional stability. Using sideways motions of the legs (figure 2), two gaits were compared: a gripping quadrilateral gait (QDP) and a triangular gait (TDP), in which the gripping waypoint has been removed (figure 3). Walking tests were performed to compare the effects of underwater substrates and waves (figure 4), dactyl shape (figure 5), friction, and gait period (table 3). The resulting QDP significantly outperformed the nongripping TDP in both speed (figure 7 and table 1) and energy cost (figures 6 and 8), table 2, providing between 20% and 30% energy savings. Outdoor testing for the speed has been conducted in grassy terrain, and the success of QDP was validated (figure 9 and table 3).

Although we had anticipated that gripping the ground might incur an energetic cost, these results instead show an energetic benefit to gripping motions. If two legs that are both contacting the ground move relative to each other, energy is lost either to work done against friction forces or to deformation of the substrate. Thus, other robots avoid inward motions of the legs. For example, in RHex class robots in sand, duty factor is reduced below 0.5 to eliminate tripod interference [39]. Here, the videos show that the two tripods are both engaged at once, but other factors are outweighing this effect. For example, touch down angle impacts can cause braking (deceleration) effects which have been essential to understanding running [48]. Even though our robot's speeds are well in the walking range (the Froude number [47] is several orders of magnitude below 0.5), the foot-substrate contact dynamics improve net distance traveled. Thus, although the COT increases in granular media relative to smooth surfaces, it appears that the benefit of inward motions outweighs the cost for our robot.

These speeds and COTs will be in improved in future work. Other legged robots have shown lower COT. For example, Shoal Legged Robot (mass 4 kg) has a walking COT of 3.7 in water [14], and Titan-XIII (mass 5.75 kg) has a walking COT of 1.76 on grass [47], suggesting that mechanical improvements and gait optimization could reduce COT perhaps

by orders of magnitude. Others have shown qualitative differences between dynamic gaits as speed increases in granular media [39]. Here, the speed of our robot is intentionally slow to reduce dynamic effects and could be increased, and the pauses in the gait removed. Additional experiments could highlight the benefits of using even smaller gait periods, where the effects of swing path on the COT could be more pronounced, as suggested by the slight increase in performance difference for the QDP gait for the smaller of the two gait periods tested. A more complete optimization could optimize the waypoints and the timing of the leg motions, perhaps using more of the workspace, varying the height of the robot, or changing the gait timing. For example, there are many possible paths and waypoint positions within the workspace with the desired conditions (e.g. enough available space for overstepping, extracting dactyl tangent to dactyl curve, etc) which could result in different touchdown angles and impact speeds, and thus affect gait performance. Such optimization might need to be performed separately on each substrate. Actuator selection is also optimizable. However, one advantage of the current high-torque actuators (which likely have a higher COT) is that the same legs can perform gripping tasks, as demonstrated in our concurrent work [49].

Nonetheless, this paper shows that future robots need not make 'to grip or not to grip' decisions when transitioning from hard to granular surfaces. On hard surfaces, the gripping QDP gait walks at the expected no-slip speed, whereas if gripping is avoided, as in the TDP gait, the speed is reduced. While walking in sand is slower, the COT of the gripping gait in sand is comparable to the COT of the nongripping on tile. Instead, rather than choosing one gait for gripping and one for walking, and trying to choose between them based on the destabilizing forces of the waves, it may be possible to choose a single gait that helps the robot be prepared for a range of natural conditions, including waves.

Acknowledgments

Data availability statement

The data that support the findings of this study will be openly available following an embargo at the followingURL/DOI: https://drive.google.com/drive/folders/1zuJxRZnzQGNLydcbcGoc6zBOMxGQyxsG?usp=sharing. 2022-04-16.

ORCID iDs

N M Graf ⓘ https://orcid.org/0000-0001-9207-0441
J E Grezmak ⓘ https://orcid.org/0000-0001-6686-5398
K A Daltorio ⓘ https://orcid.org/0000-0001-6994-1536

References

[1] Cunningham C W, Blackstone N W and Buss L W 1992 Evolution of king crabs from hermit crab ancestors *Nature* **355** 539–42

[2] Taylor J R A 2019 Biomechanics of crab skeletons on land *Integrative and Comparative Biology* vol 59 (Oxford: Oxford University Press) p E229

[3] Naleway S E, Taylor J R A, Porter M M, Meyers M A and McKittrick J 2016 Structure and mechanical properties of selected protective systems in marine organisms *Mater. Sci. Eng.* C **59** 1143–67

[4] Herreid C F and Full R J 1986 Locomotion of hermit crabs (coenobita compressus) on beach and treadmill *J. Exp. Biol.* **120** 283–96

[5] Hui C A 1992 Walking of the shore crab pachygrapsus crassipes in its two natural environments *J. Exp. Biol.* **165** 213–27

[6] Martinez M M 2001 Running in the surf: hydrodynamics of the shore crab grapsus tenuicrustatus *J. Exp. Biol.* **204** 3097–112

[7] Henry F 2006 Pumping up, the land crab way The New York Times Section F Page 3 https://www.nytimes.com/2006/04/25/science/pumping-up-the-land-crab-way.html

[8] Fluid pressure provides support—biological strategy—asknature.

[9] Taylor J R A 2018 Aquatic versus terrestrial crab skeletal support: morphology, mechanics, molting and scaling *J. Exp. Biol.* **221** jeb185421

[10] Nguyen D N, Ho N L, Dao T-P and Le Chau N 2019 Multi-objective optimization design for a sand crab-inspired compliant microgripper *Microsyst. Technol.* **25** 3991–4009

[11] Ma X, Liu Y, Liu J and Deng J 2021 Crabbot: a pole-climbing robot driven by piezoelectric stack *IEEE Trans. Robot.* **38** 765–78

[12] Cha E-Y, Jung S-P and Jung G-P 2019 Crabbot: a milli-scale crab-inspired crawling robot using double four-bar mechanism *J. Korea Robot. Soc.* **14** 245–50

[13] Greiner H, Shectman A, Won C, Elsley R and Beith P 1996 Autonomous legged underwater vehicles for near land warfare *Proc. Symp. Autonomous Underwater Vehicle Technology* (Piscataway, NJ: IEEE) pp 41–8

[14] Wang G, Chen X, Yang S, Jia P, Yan X and Xie J 2017 Subsea crab bounding gait of leg-paddle hybrid driven shoal crablike robot *Mechatronics* **48** 1–11

[15] Zhang J, Liu Q, Zhou J and Song A 2022 Crab-inspired compliant leg design method for adaptive locomotion of a multi-legged robot *Bioinspiration Biomimetics* **17** 025001

[16] Chellapurath M 2021 Bioinspired underwater legged robot for marine conservation *DOCTOR OF PHILOSOPHY in BioRobotics* SCUOLA SUPERIORE SANT'ANNA

[17] Falconer J 2013 Huge six-legged rogot crabster goes swimming IEEE Spectrum https://spectrum.ieee.org/six-legged-underwater-robot-crabster

[18] Krummel G, Kaipa K N and Gupta S K 2014 A horseshoe crab inspired surf zone robot with righting capabilities *Int. Design Engineering Technical Conf. Computers and Information in Engineering Conf.* vol 46360 (American Society of Mechanical Engineers) pp

[19] Wile G D, Daltorio K A, Diller E D, Palmer L R, Gorb S N, Ritzmann R E and Quinn R D 2008 Screenbot: walking inverted using distributed inward gripping *2008 IEEE/RSJ Int. Conf. Intelligent Robots and Systems* (Piscataway, NJ: IEEE) pp 1513–8

[20] Hawkes E W *et al* 2013 Dynamic surface grasping with directional adhesion *2013 IEEE/RSJ Int. Conf. Intelligent Robots and Systems* (Piscataway, NJ: IEEE) pp 5487–93

[21] Palmer L R III, Diller E and Quinn R D 2014 Toward gravity-independent climbing using a biologically inspired distributed inward gripping strategy *IEEE/ASME Trans. Mechatron.* **20** 631–40

[22] Wang S, Jiang H, Huh T M, Sun D, Wilson R, Miller M, Roderick W R T, Stuart H S and Cutkosky M R 2019 Spinyhand: contact load sharing for a human-scale climbing robot *J. Mech. Robot.* **11** 031009

[23] Ruotolo W, Roig F S and Cutkosky M R 2019 Load-sharing in soft and spiny paws for a large climbing robot *IEEE Robot. Autom. Lett.* **4** 1439–46

[24] Xie C, Wu X and Wang X 2019 A three-row opposed gripping mechanism with bioinspired spiny toes for wall-climbing robots *J. Bionic Eng.* **16** 994–1006

[25] Hassan M, Rashid M and Abdulaali A 2019 Design and implementation of hybrid-climbing legged robot *Iraqi J. Electr. Electron. Eng.* **15** 37–46

[26] Liu J, Xu L, Chen S, Xu H, Cheng G, Li T and Yang Q 2019 Design and realization of a bio-inspired wall climbing robot for rough wall surfaces *Int. Conf. Intelligent Robotics and Applications* (Berlin: Springer) pp 47–59

[27] Li X, Cao H, Feng S and Xie C 2020 Structure design and mobility analysis of a climbing robot *J. Phys.: Conf. Ser.* **1550** 022015

[28] Xu F, Meng F, Jiang Q and Peng G 2020 Grappling claws for a robot to climb rough wall surfaces: mechanical design, grasping algorithm, and experiments *Robot. Autonom. Syst.* **128** 103501

[29] Graf N M, Behr A M and Daltorio K A 2021 Dactyls and inward gripping stance for amphibious crab-like robots on sand *Bioinspiration Biomimetics* **16** 026021

[30] Graf N M, Behr A M and Daltorio K A 2019 Crab-like hexapod feet for amphibious walking in sand and waves *Conf. Biomimetic and Biohybrid Systems* (Berlin: Springer) pp 158–70

[31] Ries E M 2022 Crab-like dactyl testing in two beach sands and play sand *PhD Thesis* Case Western Reserve University

[32] Chen Y, Grezmak J E, Graf N M and Daltorio K A 2022 Sideways crab-walking is faster and more efficient than forward walking for a hexapod robot *Bioinspiration Biomimetics* **17** 046001

[33] Yang K, Li Y, Zhou L and Rong X 2019 Energy efficient foot trajectory of trot motion for hydraulic quadruped robot *Energies* **12** 2514

[34] Kim T-J, So B, Kwon O and Park S 2010 The energy minimization algorithm using foot rotation for hydraulic actuated quadruped walking robot with redundancy *ISR*

2010 (41st Int. Symp. Robotics) and ROBOTIK 2010 (6th German Conf. Robotics) pp 1–6

[35] Gao H, Liu Y, Ding L, Liu G, Deng Z, Liu Y and Yu H 2019 Low impact force and energy consumption motion planning for hexapod robot with passive compliant ankles *J. Intell. Robot. Syst.* **94** 349–70

[36] Bergés P and Bowling A 2006 Rebound, slip, and compliance in the modeling and analysis of discrete impacts in legged locomotion *J. Vib. Control* **12** 1407–30

[37] Mahapatra A, Roy S S and Pratihar D K 2016 Inverse dynamics and feet-terrain collision model for optimal distribution of the contact forces during crab motion of a hexapod robot *CAD/CAM, Robotics and Factories of the Future* (Berlin: Springer) pp 85–95

[38] Mahapatra A, Roy S S and Pratihar D K 2019 Study on feet forces' distributions, energy consumption and dynamic stability measure of hexapod robot during crab walking *Appl. Math. Modell.* **65** 717–44

[39] Li C, Umbanhowar P B, Komsuoglu H, Koditschek D E and Goldman D I 2009 Sensitive dependence of the motion of a legged robot on granular media *Proc. Natl Acad. Sci. USA* **106** 3029–34

[40] Wu X A, Huh T M, Sabin A, Suresh S A and Cutkosky M R 2019 Tactile sensing and terrain-based gait control for small legged robots *IEEE Trans. Robot.* **36** 15–27

[41] Pullinz A, Fearing R S and Goldman D I 2013 Walking and running on yielding and fluidizing ground *Robotics Science and Systems VIII* 345

[42] Mahapatra A, Roy S S and Pratihar D K 2020 Optimal feet-forces' and torque distributions of six-legged robot maneuvering on various terrains *Robotica* **38** 1041–63

[43] Chen Y, Clifton G, Graf N M, Duarnd K, Taylor J, Gong Y, Grezmak J E and Daltorio K 2022 Optimal planar leg geometry for idealized rocky terrain in robots and crabs *Bioinspiration & Biomimetics*

[44] Alexander R M 1984 The gaits of bipedal and quadrupedal animals *Int. J. Robot. Res.* **3** 49–59

[45] Nishii J 1998 Gait pattern and energetic cost in hexapods *Proc. 20th Annual Int. Conf. IEEE Engineering in Medicine and Biology Society. Volume 20 Biomedical Engineering Towards the Year 2000 and Beyond (Cat. No. 98CH36286)* vol 5 (Piscataway, NJ: IEEE) pp 2430–3

[46] Nishii J 2000 Legged insects select the optimal locomotor pattern based on the energetic cost *Biol. Cybern.* **83** 435–42

[47] Kitano S, Hirose S, Horigome A and Endo G 2016 Titan-XIII: sprawling-type quadruped robot with ability of fast and energy-efficient walking *ROBOMECH J.* **3** 8

[48] Raibert M, Chepponis M and Brown H 1986 Running on four legs as though they were one *IEEE J. Robot. Automat.* **2** 70–82

[49] Gong Y, Behr A M, Graf N M, Chen K, Gong Z and Daltorio K A 2022 A walking claw for tethered object retrieval. *ASME the Journal of Mechanisms and Robotics* (accepted)